Non-Singular Fixed-Time Sliding Mode Control for Unknown-Dynamics Manipulators Interacting with Environment

Haiyi Kong[1], Guang Li[1], Chenguang Yang[2*]
[1] School of Engineering and Materials Science, Queen Mary University of London, Mile End Road, London E1 4NS, UK.
[2] Bristol Robotics Laboratory, University of the West of England, Bristol, BS16 1QY, UK.
*Corresponding author: cyang@ieee.org

***Abstract*—In this paper, a robust fixed-time controller is designed for manipulators with unknown dynamics while interacting with environment. To realize compliance of the manipulator to the environment, an admittance model is adopted in the system. In the controller design, a non-singular sliding mode torque is introduced to achieve fixed-time convergence of the system state, so that the system has better tracking performance and faster response to external interaction than that using the traditional terminal sliding mode method. As for the unknown dynamics of the manipulator, radial basis function neural networks are developed to approximate the parameters in the dynamics. At last, simulation studies are conducted to verify the effectiveness of the proposed method.**

***Index Terms*—Admittance control, non-singular sliding mode control, fixed-time convergence, neural network.**

I. Introduction

Manipulators have received great attention in many fields due to their high degree of flexibility, such as industry, transportation, and medicine [1]- [2]. With the increasing complexity of application scenarios, higher requirements are put forward for manipulators, among which the ability to deal with the external environment is important.

Compliance is a way to interact with environment for manipulators, which can greatly improve manipulators' safety. During working process, if the manipulator is suddenly blocked by an external force, compliance can drive the manipulator to move along external force instead of generating larger torque against the environment [3]. When the external force is withdrawn, the manipulator will resume tracking the original trajectory. To realize the relationship between the environmental interaction position and interaction force, Mason proposed the admittance model in 1981 [4]. In [5]- [6], the adaptive admittance control is adopted to realize compliant behavior for redundant manipulators. In [7]- [8], an admittance model is employed in the system for cooperation between multi-manipulators.

When the manipulator is in contact with the environment, it will inevitably introduce undesirable interference torques, such as frictional torque and external disturbance. As for coping with external disturbance and system parameter perturbations, sliding mode control is a powerful method, which can effectively improve the robustness of the system [9]. In the early stage, linear hyperplane was used in the sliding mode control, where the system state can realize asymptotic stability [10]. Because the convergence time is infinite in theory, which is not realistic in the actual control. Hence, in this context, terminal sliding mode (TSM) was developed for achieving finite-time convergence [11]. However, traditional TSM controllers all suffer from the singularity problem. To tackle this problem, [12] proposed to switch the sliding mode between TSM and linear hyperplane, and [13] specified a non-singular open region. On the other hand, the convergence time of the finite-time TSM control depends on the initial states of the closed-loop system, which cannot be obtained beforehand. This drawback can be overcome by the recently upgraded TSM, that is fixed-time TSM control, where the settling time is uniformly bounded by a fixed time and independent of initial system states [14].

For general manipulator systems, computed torque control is usually used to achieve desired tracking performance [15]. However, the system's performance largely depends on the fidelity of the system model. In practice, accurate models of manipulators are difficult to obtain. In this context, much attention has been drawn to neural network, which can be used to approximate inaccurate or unknown dynamics of manipulators [16]. Radial basis function neural network (RBFNN) is one of the commonly used neural networks [17]. Because of its simple structure and strong generalization ability, RBFNN is especially suitable for systems requiring high real-time performance.

In this paper, we design a robust non-singular fixed-time controller for manipulators interacting with environment, where an admittance model is introduced to realize compliant motion. In the control design, a non-singular fixed-time switching manifold is employed to achieve desired fixed-time convergence for the system state, which results in better tracking performance of the system and faster response to external interaction than the system using traditional TSM controller. Meanwhile, RBFNN is employed to approximate

This work was supported by China Scholarship Council and Queen Mary University of London.

the unknown parameters in the dynamics. Simulation results are given to prove the effectiveness of the proposed method.

II. Preliminaries

A. System Dynamics

The dynamic model of a $\mathcal{N}$-joint manipulator can be expressed as

$$\mathcal{M}_a(q)\ddot{q} + \mathcal{C}_a(q,\dot{q})\dot{q} + \mathcal{G}_a(q) + d = \tau + \mathcal{J}^T\mathcal{F}_e \tag{1}$$

where $\ddot{q}$, $\dot{q}$, $q \in \mathbb{R}^{\mathcal{N}}$ represent acceleration, velocity and angle of the manipulator, respectively. $\mathcal{M}_a \in \mathbb{R}^{\mathcal{N}\times\mathcal{N}}$ stands for the inertia matrix in symmetric positive definite. $\mathcal{G}_a \in \mathbb{R}^{\mathcal{N}}$ represents the vector of gravity. $\tau \in \mathbb{R}^{\mathcal{N}}$ is the joint torque representing the control input of the system. The interaction force between the environment and the end-effector of the manipulator is expressed as $\mathcal{F}_e \in \mathbb{R}^{\mathcal{N}}$, which can be acquired by force sensor. $\mathcal{J}^T \in \mathbb{R}^{\mathcal{N}\times\mathcal{N}}$ is the transpose of the Jacobian matrix corresponding to the mapping from joint velocity to workspace velocity. d represents the external disturbance, which is assumed to be bounded $\|d\| \leq d_m$. $\mathcal{C}_a \in \mathbb{R}^{\mathcal{N}\times\mathcal{N}}$ denotes the Coriolis matrix, which is chosen to satisfy

$$\dot{\mathcal{M}}_a(q) = \mathcal{C}_a(q,\dot{q}) + \mathcal{C}_a^T(q,\dot{q}) \tag{2}$$

The forward kinematic model of the manipulation is

$$\mathtt{x} = \Xi(q) \tag{3}$$

where $\mathtt{x} \in \mathbb{R}^{\mathcal{N}_c}$ is the pose of end-effector in Cartesian space with dimension N_c. Taking the first and second derivative of (3) yields

$$\dot{\mathtt{x}} = \mathcal{J}(q)\dot{q} \tag{4}$$

$$\ddot{\mathtt{x}} = \dot{\mathcal{J}}(q)\dot{q} + \mathcal{J}(q)\ddot{q} \tag{5}$$

B. Admittance Control

To achieve compliant motion of the manipulator when its end-effector follows the reference trajectory and interacts constantly with the environment, the reference position should be regulated accordingly. Admittance control is proposed for this purpose, that is, to maintain desired force contact by adjusting position. Commonly, the applied admittance model in the Cartesian space is chosen as

$$\mathcal{D}_A(\ddot{\mathtt{x}}_r - \ddot{\mathtt{x}}_d) + \mathcal{C}_A(\dot{\mathtt{x}}_r - \dot{\mathtt{x}}_d) + \mathcal{G}_A(\mathtt{x}_r - \mathtt{x}_d) = -\mathcal{F}_e \tag{6}$$

where $\mathtt{x}_d$ is the desired position in the original trajectory, $\mathtt{x}_r$ is the reference position produced by admittance model. (6) is the typical mass-damping-stiffness model, in which $\mathcal{D}_A$, $\mathcal{C}_A$ and $\mathcal{G}_A$ are positive diagonal matrices. Based on (4) and (5), the admittance model (6) can be transformed into joint space

$$\begin{aligned}\mathcal{D}_A\mathcal{J}(q)(\ddot{q}_r - \ddot{q}_d) + \Big(\mathcal{D}_A\dot{\mathcal{J}}(q) + \mathcal{C}_A\mathcal{J}(q)\Big)(\dot{q}_r - \dot{q}_d) \\ + \mathcal{G}_A(\Xi(q_r) - \Xi(q_d)) = -\mathcal{J}^{-T}(q)\tau_e\end{aligned} \tag{7}$$

where τ_e is the joint torque produced by the interaction with environment and $\tau_e = \mathcal{J}^T(q)\mathcal{F}_e$.

C. RBF Neural Network

RBFNN has superior generalization ability that can approximate arbitrary linear or nonlinear function. The activation function commonly uses the Gaussian function:

$$\mathcal{Y}_j(x) = \exp(\|x - \sigma_j\|^2/\varrho_j^2), \quad j = 1,2,\ldots,m \tag{8}$$

where m denotes the corresponding number of neuron, $\mathcal{Y}_j$ is the output of hidden layer, and $\mathcal{Y} = [\mathcal{Y}_1, \mathcal{Y}_2, \ldots, \mathcal{Y}_m]^T \in \mathbb{R}^m$. $x \in \Omega_x \subset \mathbb{R}^l$ is the l-dimension input of the neural network. $\varrho_j \in \mathbb{R}$ and $\sigma_j \in \mathbb{R}^l$ represent the width and center of Gaussian function of the j-th hidden node, respectively. $\|\cdot\|$ is the norm of Euclidian distance.

For arbitrary continuous vector function $\mathfrak{f}(x) \in \mathbb{R}^n$ approximating by RBFNN, it can be written in the form of

$$\mathfrak{f}_i(x) = \mathcal{W}_i^{*T}\mathcal{Y}(x) + \epsilon_i(x), \ i = 1,2,\ldots,n \tag{9}$$

where ϵ_i stands for the small approximation error and satisfies $\epsilon_i \leq \bar{\epsilon}$, $\bar{\epsilon}$ is the known upper bound. We define $\epsilon = [\epsilon_1, \epsilon_2, \ldots, \epsilon_n]^T$ and $\mathcal{W}^* = [\mathcal{W}_1^*, \mathcal{W}_2^*, \ldots, \mathcal{W}_n^*]^T \in \mathbb{R}^{m\times n}$ where $\mathcal{W}^*$ represents the ideal weight of neural network.

Take $\hat{\mathcal{W}}$ as the estimation of $\mathcal{W}^*$. Correspondingly, we can denote the estimation of the continuous function as

$$\hat{\mathfrak{f}}_i(x) = \hat{\mathcal{W}}_i^T\mathcal{Y}(x), \ i = 1,2,\ldots,n \tag{10}$$

where $\hat{\mathfrak{f}}(x) = [\hat{\mathfrak{f}}_1(x), \hat{\mathfrak{f}}_2(x), \ldots, \hat{\mathfrak{f}}_n(x)]^T \in \mathbb{R}^n$ and $\hat{\mathcal{W}} = [\hat{\mathcal{W}}_1, \hat{\mathcal{W}}_2, \ldots, \hat{\mathcal{W}}_n]^T \in \mathbb{R}^{m\times n}$. This is usually what we can obtain using RBFNN in practice.

D. Fundamental Facts

Consider a nonlinear system:

$$\dot{x}(t) = \ell(x(t)) \tag{11}$$

whose initial value is x_0. $\ell(\cdot)$ represents a nonlinear mapping. System (11) can be discontinuous and assumed to have a unique solution in forward time for arbitrary initial states [18].

Lemma 1: [19] The origin of the nonlinear system (11) is said to be fixed-time stable with setting time $\mathcal{T}$ if there exists a Lyapunov function $\mathcal{V}(x)$ and satisfies

$$\dot{\mathcal{V}} \leq -\kappa\mathcal{V}^{\gamma_1} - \varsigma\mathcal{V}^{\gamma_2} + \varpi \tag{12}$$

where scalars $\kappa, \varsigma > 0$, $\gamma_1 \in (0,1)$, $\gamma_2 \in (1,\infty)$, $\varpi \in (0,\infty)$. The convergence time $\mathcal{T}$ is bounded by

$$\mathcal{T} \leq \frac{1}{\kappa}\frac{1}{1-\gamma_1} + \frac{1}{\varsigma}\frac{1}{\gamma_2 - 1} \tag{13}$$

Lemma 2: [20] For any $x_i \in \mathbb{R}$, $i = 1,2,\ldots,n$, the following inequalities hold:

$$\sum_{i=1}^{n} |\ x_i\ |^{\gamma_1} \geq (\sum_{i=1}^{n} |\ x_i\ |)^{\gamma_1}, \quad \text{if } \gamma_1 \in (0,1] \tag{14}$$

$$\sum_{i=1}^{n} |\ x_i\ |^{\gamma_2} \geq n^{1-\gamma_2}(\sum_{i=1}^{n} |\ x_i\ |)^{\gamma_2}, \quad \text{if } \gamma_2 \in (1,\infty) \tag{15}$$

To facilitate the development of the following section, a new continuous function is defined as

$$\mathrm{sgn}^{\alpha}(x) = |\ x\ |^{\alpha}\ \mathrm{sign}(x) \tag{16}$$

where $\mathrm{sign}(\cdot)$ is the standard signum and $\alpha \geq 0$ is a constant.

III. Control System Design and Stability Analysis

A. Non-Singular Switching Manifold

Traditional TSM controllers face the singularity problem. Because the control law contains negative exponent of the system state, a singularity occurs when the system state reaches zero. In this paper, a non-singular switching manifold is introduced to avoid singularity.

Firstly, define two important parameters:

$$\phi = \frac{-1 - \ln \vartheta}{\rho - \vartheta \ln \vartheta} \qquad \psi = \frac{\vartheta^{2\rho-2}}{\rho - \vartheta \ln \vartheta}$$

Then, a nonlinear function $\hbar$ is introduced [14]:

$$\hbar = \begin{cases} \phi \operatorname{sgn}^{\rho+1}(x) + \psi \vartheta^{|x|} x, & \text{if } \mid x \mid \leq \vartheta \\ \operatorname{sgn}^{\rho}(x), & \text{if } \mid x \mid > \vartheta \end{cases} \tag{17}$$

Take the first derivative of function (17), we have:

$$\Im = \begin{cases} (\phi\rho + \phi) \mid x \mid^{\rho} + \psi(\mid x \mid \ln \vartheta + 1)\vartheta^{|x|}, & \text{if } \mid x \mid \leq \vartheta \\ \rho \mid x \mid^{\rho-1}, & \text{if } \mid x \mid > \vartheta \end{cases} \tag{18}$$

where scalars $\rho > 0$, $\vartheta \in (0, \exp(-1))$ and satisfy the relationship $\rho = 1 - \vartheta$. It is worth noting that the selection of ϕ and ψ needs to guarantee the continuity of function $\hbar$ and $\Im$ when $\mid x \mid = \vartheta$.

Define the tracking error as

$$e := q_r - q \tag{19}$$

where $q_r \in \mathbb{R}^{\mathcal{N}}$ is the desired position, $e = [e_1, e_2, \ldots, e_{\mathcal{N}}] \in \mathbb{R}^{\mathcal{N}}$. Define the following vectors and matrices:

$$\begin{aligned} \mathcal{H}(e) &= [\hbar(e_1), \hbar(e_2), \ldots, \hbar(e_{\mathcal{N}})]^T \in \mathbb{R}^{\mathcal{N}} \\ \Gamma(e) &= \operatorname{diag}\{\Im(e_i)\} \in \mathbb{R}^{\mathcal{N}\times\mathcal{N}},\ i = 1, 2, \ldots, \mathcal{N} \\ \mathcal{S}\operatorname{sgn}^{\alpha}(e) &= [\operatorname{sgn}^{\alpha}(e_1), \operatorname{sgn}^{\alpha}(e_2), \ldots, \operatorname{sgn}^{\alpha}(e_{\mathcal{N}})]^T \in \mathbb{R}^{\mathcal{N}} \\ \mathcal{D}^{\alpha-1}(e) &= \operatorname{diag}\{\mid e_i \mid^{\alpha-1}\} \in \mathbb{R}^{\mathcal{N}\times\mathcal{N}},\ i = 1, 2, \ldots, \mathcal{N} \end{aligned}$$

where $\operatorname{diag}\{\cdot\}$ denotes the diagonal matrix. Then, a non-singular switching manifold can be designed as [14]

$$\mathcal{S} = \dot{e} + \mathcal{K}_1 \mathcal{H}(e) + \mathcal{K}_2 \mathcal{S}\operatorname{sgn}^{\alpha}(e) \tag{20}$$

where $\mathcal{S} = [\mathcal{S}_1, \mathcal{S}_2, \ldots, \mathcal{S}_{\mathcal{N}}]^T \in \mathbb{R}^{\mathcal{N}}$, constant $\alpha > 1$, matrices $\mathcal{K}_1$, $\mathcal{K}_2 \in \mathbb{R}^{\mathcal{N}\times\mathcal{N}}$ are of positive diagonal definition. Upon differentiating $\mathcal{S}$ with respect to time, we can obtain:

$$\dot{\mathcal{S}} = \ddot{e} + \mathcal{K}_1 \Gamma(e)\dot{e} + \alpha \mathcal{K}_2 \mathcal{D}^{\alpha-1}(e)\dot{e} \tag{21}$$

B. Non-Singular Fixed-Time Controller

Based on the designed switching manifold (20), a robust non-singular fixed-time controller is proposed in this section.

Substituting (21) and the second derivative of the tracking error (19) into the dynamic manipulator model (1), we can acquire

$$\begin{aligned} \mathcal{M}_a \dot{\mathcal{S}} =& \mathcal{M}_a \ddot{q}_r + \mathcal{M}_a \mathcal{K}_1 \Gamma \dot{e} + \alpha \mathcal{M}_a \mathcal{K}_2 \mathcal{D}^{\alpha-1} \dot{e} + \mathcal{C}_a \dot{q} \\ &+ \mathcal{G}_a - \tau - \tau_e + d \end{aligned} \tag{22}$$

To simplify (22), we define a new variable η, where

$$\eta := \mathcal{S} + \dot{q} \tag{23}$$

Thus, the closed-loop error dynamic model (22) can be rewritten as

$$\mathcal{M}_a \dot{\mathcal{S}} + \mathcal{C}_a \mathcal{S} = \mathcal{M}_a \dot{\eta} + \mathcal{C}_a \eta + \mathcal{G}_a - \tau - \tau_e + d \tag{24}$$

Based on (24), we design the non-singular fixed-time controller as

$$\tau_0 = \mathcal{K}_3 \mathcal{S}\operatorname{sgn}^{\beta_1}(\mathcal{S}) + \mathcal{K}_4 \mathcal{S}\operatorname{sgn}^{\beta_2}(\mathcal{S}) \tag{25}$$

$$\tau_1 = \mathcal{K}_5 \mathcal{S}\operatorname{sgn}(\mathcal{S}) + \mathcal{K}_6 \mathcal{S}\operatorname{sgn}^{0}(\mathcal{S}) \tag{26}$$

$$\tau = \hat{\mathcal{M}}_a \eta + \hat{\mathcal{C}}_a \dot{q} + \hat{\mathcal{G}}_a - \tau_e + \tau_0 + \tau_1 \tag{27}$$

where τ_0 is the fixed-time sliding mode torque. The settling time of the sliding variable $\mathcal{S}$ to the origin is determined by the positive diagonal matrices $\mathcal{K}_3$, $\mathcal{K}_4 \in \mathbb{R}^{\mathcal{N}\times\mathcal{N}}$ and the positive parameters $\beta_1 \in (0, 1)$, $\beta_2 \in (1, \infty)$ in τ_0. $\mathcal{K}_5 \in \mathbb{R}^{\mathcal{N}\times\mathcal{N}}$ is the factor related to the uniformly ultimately boundedness (UUB) of the system. $\mathcal{K}_6 \in \mathbb{R}^{\mathcal{N}}$ is the coefficient diagonal matrix of the robust term and its diagonal element satisfies $\mathcal{K}_{6i} \geq \mid \mathcal{E}_i \mid$, where $\mathcal{E} = d + \epsilon_{\mathcal{M}}\dot{\eta} + \epsilon_{\mathcal{C}}\eta + \epsilon_{\mathcal{G}}$ and $\epsilon_{\mathcal{M}}$, $\epsilon_{\mathcal{C}}$, $\epsilon_{\mathcal{G}}$ are the approximation errors. τ_e is directly acquired from the sensor. $\hat{\mathcal{M}}_a$, $\hat{\mathcal{C}}_a$, and $\hat{\mathcal{G}}_a$ represent the estimation of $\mathcal{M}_a$, $\mathcal{C}_a$ and $\mathcal{G}_a$ using RBFNN, which can be expressed as $\hat{\mathcal{M}}_a = \hat{\mathcal{W}}_M \mathcal{Y}_M$, $\hat{\mathcal{C}}_a = \hat{\mathcal{W}}_C \mathcal{Y}_C$, and $\hat{\mathcal{G}}_a = \hat{\mathcal{W}}_G \mathcal{Y}_G$. The updating law is designed as

$$\begin{aligned} \dot{\hat{\mathcal{W}}}_{Mi} &= \mathcal{P}_{Mi}(\mathcal{Y}_{Mi}\dot{\eta}\mathcal{S}_i - \varepsilon_{Mi}\hat{\mathcal{W}}_{Mi}) \\ \dot{\hat{\mathcal{W}}}_{Ci} &= \mathcal{P}_{Ci}(\mathcal{Y}_{Ci}\eta\mathcal{S}_i - \varepsilon_{Ci}\hat{\mathcal{W}}_{Ci}) \\ \dot{\hat{\mathcal{W}}}_{Gi} &= \mathcal{P}_{Gi}(\mathcal{Y}_{Gi}\mathcal{S}_i - \varepsilon_{Gi}\hat{\mathcal{W}}_{Gi}),\ i = 1, \ldots, \mathcal{N} \end{aligned} \tag{28}$$

where $\mathcal{P}_{Mi}$, $\mathcal{P}_{Ci}$, $\mathcal{P}_{Gi}$ matrices are positive diagonal definition, ε_{Mi}, ε_{Ci}, ε_{Gi} are small positive constants for disturbance.

Under the control of (27), the system state can firstly reach the switching manifold (20) that is $\mathcal{S} = 0$ within the fixed time $\mathcal{T}_1$. Subsequently, along the switching manifold, the system state enters the small domain of the origin $\Omega = \{e_i \mid \mid e_i \mid \leq \vartheta\}$ within the fixed time $\mathcal{T}_2$ and asymptotically gets to the origin in the end. According to *Lemma 1*, the fixed-time $\mathcal{T}_1$ and $\mathcal{T}_2$ can be calculated, which will be given in the next section.

C. Stability Analysis

Theorem 1: Upon introducing the non-singular fixed-time controller to the manipulator system (1), the tracking error of the system can achieve fixed-time convergence regardless of the initial conditions.

Proof: The fixed-time convergence analysis of the system can be divided into two stages. The fist stage is to prove $\mathcal{S} = 0$, where the system state reaches the switching manifold within $\mathcal{T}_1$. The second stage is to prove that the tracking error e converges to the small domain Ω within $\mathcal{T}_2$, then asymptotically converges to the origin.

stage 1:

Construct the Lyapunov function candidate as

$$\mathcal{V} = \frac{1}{2}\mathcal{S}^T\mathcal{M}_a\mathcal{S} + \frac{1}{2}\sum_{i=0}^{\mathcal{N}}\tilde{\mathcal{W}}_{Mi}^T\mathcal{P}_{Mi}^{-1}\tilde{\mathcal{W}}_{Mi} + \frac{1}{2}\sum_{i=0}^{\mathcal{N}}\tilde{\mathcal{W}}_{Ci}^T\mathcal{P}_{Ci}^{-1}\tilde{\mathcal{W}}_{Ci} + \frac{1}{2}\sum_{i=0}^{\mathcal{N}}\tilde{\mathcal{W}}_{Gi}^T\mathcal{P}_{Gi}^{-1}\tilde{\mathcal{W}}_{Gi} \tag{29}$$

where $\tilde{\mathcal{W}}_{(\cdot i)}$ is the weight estimation error and $\tilde{\mathcal{W}}_{(\cdot i)} = \mathcal{W}_{(\cdot i)}^* - \hat{\mathcal{W}}_{(\cdot i)}$. Taking the derivative of (29), then substituting (2) and (24)- (28), we can obtain:

$$\begin{aligned}\dot{\mathcal{V}} =& \mathcal{S}^T[-\mathcal{K}_3\mathcal{S}\mathrm{gn}^{\beta_1}(\mathcal{S}) - \mathcal{K}_4\mathcal{S}\mathrm{gn}^{\beta_2}(\mathcal{S}) - \mathcal{K}_5\mathcal{S}\mathrm{gn}(\mathcal{S}) \\ &- \mathcal{K}_6\mathcal{S}\mathrm{gn}^0(\mathcal{S})] + \mathcal{S}^T\mathcal{E} + \sum_{i=0}^{\mathcal{N}}\varepsilon_{Mi}\tilde{\mathcal{W}}_{Mi}^T\hat{\mathcal{W}}_{Mi} \\ &+ \sum_{i=0}^{\mathcal{N}}\varepsilon_{Ci}\tilde{\mathcal{W}}_{Ci}^T\hat{\mathcal{W}}_{Ci} + \sum_{i=0}^{\mathcal{N}}\varepsilon_{Gi}\tilde{\mathcal{W}}_{Gi}^T\hat{\mathcal{W}}_{Gi}\end{aligned} \tag{30}$$

Since

$$\sum_{i=0}^{\mathcal{N}}\varepsilon_{(\cdot i)}\tilde{\mathcal{W}}_{(\cdot i)}^T\hat{\mathcal{W}}_{(\cdot i)} \leq \sum_{i=0}^{\mathcal{N}}\frac{\varepsilon_{(\cdot i)}}{2}\|\mathcal{W}_{(\cdot i)}^*\|^2 - \sum_{i=0}^{\mathcal{N}}\frac{\varepsilon_{(\cdot i)}}{2}\|\tilde{\mathcal{W}}_{(\cdot i)}\|^2$$

(30) can be transformed into

$$\begin{aligned}\dot{\mathcal{V}} \leq& -\sum_{i=0}^{\mathcal{N}}\frac{2\lambda_{\min}\{\mathcal{K}_5\}}{\lambda_{\max}\{\mathcal{M}_a\}}\frac{1}{2}\lambda_{\max}\{\mathcal{M}_a\} \mid \mathcal{S}_i \mid^2 \\ &- \sum_{i=0}^{\mathcal{N}}\frac{\varepsilon_{Mi}}{\lambda_{\max}\{\mathcal{P}_{Mi}^{-1}\}}\frac{1}{2}\lambda_{\max}\{\mathcal{P}_{Mi}^{-1}\}\|\tilde{\mathcal{W}}_{Mi}\|^2 \\ &- \sum_{i=0}^{\mathcal{N}}\frac{\varepsilon_{Ci}}{\lambda_{\max}\{\mathcal{P}_{Ci}^{-1}\}}\frac{1}{2}\lambda_{\max}\{\mathcal{P}_{Ci}^{-1}\}\|\tilde{\mathcal{W}}_{Ci}\|^2 \\ &- \sum_{i=0}^{\mathcal{N}}\frac{\varepsilon_{Gi}}{\lambda_{\max}\{\mathcal{P}_{Gi}^{-1}\}}\frac{1}{2}\lambda_{\max}\{\mathcal{P}_{Gi}^{-1}\}\|\tilde{\mathcal{W}}_{Gi}\|^2 + \zeta_1 \\ \leq& -\varphi_1\mathcal{V} + \zeta_1\end{aligned} \tag{31}$$

where $\lambda_{\max}\{\cdot\}$ and $\lambda_{\min}\{\cdot\}$ denote the largest and smallest eigenvalue of the matrix, respectively. $\zeta_1 = \sum_{i=0}^{\mathcal{N}}\frac{\varepsilon_{Mi}}{2}\|\mathcal{W}_{Mi}^*\|^2 + \sum_{i=0}^{\mathcal{N}}\frac{\varepsilon_{Ci}}{2}\|\mathcal{W}_{Ci}^*\|^2 + \sum_{i=0}^{\mathcal{N}}\frac{\varepsilon_{Gi}}{2}\|\mathcal{W}_{Gi}^*\|^2$, $\varphi_1 = \min\{\frac{2\lambda_{\min}\{\mathcal{K}_5\}}{\lambda_{\max}\{\mathcal{M}_a\}}, \frac{\varepsilon_{Mi}}{\lambda_{\max}\{\mathcal{P}_{Mi}^{-1}\}}, \frac{\varepsilon_{Ci}}{\lambda_{\max}\{\mathcal{P}_{Ci}^{-1}\}}, \frac{\varepsilon_{Gi}}{\lambda_{\max}\{\mathcal{P}_{Gi}^{-1}\}}\}$, $\min\{\cdot\}$ represents the operation of taking the minimum value. According to Lemma 22 in [21], we can derive that

$$\mathcal{V} \leq \mathcal{V}(0)e^{-\varphi_1 t} + \frac{\zeta_1}{\varphi_1}(1 - e^{-\varphi_1 t}),\ t \geq 0 \tag{32}$$

Remark 1: For the Lyapunov function (29) $\mathcal{V} > 0$ and its first derivative satisfying $\dot{\mathcal{V}} \leq -\varphi_1\mathcal{V} + \zeta_1$, we can acquire its maximal solution expressed as (32). Since $\mathcal{V}(0)$ is bounded, we can derive that $\mathcal{S}$, $\tilde{\mathcal{W}}_{(\cdot i)}$ and $\hat{\mathcal{W}}_{(\cdot i)}$ are bounded.

Based on (30), we can develop

$$\begin{aligned}\dot{\mathcal{V}} \leq& -\mathcal{S}^T\mathcal{K}_3\mathcal{S}\mathrm{gn}^{\beta_1}(\mathcal{S}) - \mathcal{S}^T\mathcal{K}_4\mathcal{S}\mathrm{gn}^{\beta_2}(\mathcal{S}) + \sum_{i=0}^{\mathcal{N}}(-\mathcal{K}_{6i}* \\ &\|\tilde{\mathcal{W}}_{Mi}\|^{1+\beta_1} - \mathcal{K}_{7i}\|\tilde{\mathcal{W}}_{Mi}\|^{1+\beta_2} - \mathcal{K}_{8i}\|\tilde{\mathcal{W}}_{Ci}\|^{1+\beta_1} \\ &- \mathcal{K}_{9i}\|\tilde{\mathcal{W}}_{Ci}\|^{1+\beta_2} - \mathcal{K}_{10i}\|\tilde{\mathcal{W}}_{Gi}\|^{1+\beta_1} \\ &- \mathcal{K}_{11i}\|\tilde{\mathcal{W}}_{Gi}\|^{1+\beta_2}) + \zeta_2\end{aligned} \tag{33}$$

where $\zeta_2 = \sum_{i=0}^{\mathcal{N}}(\frac{\varepsilon_{Mi}}{2}\|\mathcal{W}_{Mi}^*\|^2 + \frac{\varepsilon_{Ci}}{2}\|\mathcal{W}_{Ci}^*\|^2 + \frac{\varepsilon_{Gi}}{2}\|\mathcal{W}_{Gi}^*\|^2 + \mathcal{K}_{6i}\|\tilde{\mathcal{W}}_i\|^{1+\beta_1} + \mathcal{K}_{7i}\|\tilde{\mathcal{W}}_i\|^{1+\beta_2} + \mathcal{K}_{8i}\|\tilde{\mathcal{W}}_{Ci}\|^{1+\beta_1} + \mathcal{K}_{9i}\|\tilde{\mathcal{W}}_{Ci}\|^{1+\beta_2} + \mathcal{K}_{10i}\|\tilde{\mathcal{W}}_{Gi}\|^{1+\beta_1} + \mathcal{K}_{11i}\|\tilde{\mathcal{W}}_{Gi}\|^{1+\beta_2})$.

Utilizing *Lemma 2*, $\mathcal{V}$ can be transformed into

$$\begin{aligned}\dot{\mathcal{V}} \leq& -\sum_{i=0}^{\mathcal{N}}\frac{\lambda_{\min}\{\mathcal{K}_3\}}{(\frac{1}{2}\lambda_{\min}\{\mathcal{M}_a\})^{\frac{1+\beta_1}{2}}}(\frac{1}{2}\lambda_{\min}\{\mathcal{M}_a\} \mid \mathcal{S}_i \mid^2)^{\frac{1+\beta_1}{2}} \\ &- \sum_{i=0}^{\mathcal{N}}\frac{\lambda_{\min}\{\mathcal{K}_4\}}{(\frac{1}{2}\lambda_{\min}\{\mathcal{M}_a\})^{\frac{1+\beta_2}{2}}}(\frac{1}{2}\lambda_{\min}\{\mathcal{M}_a\} \mid \mathcal{S}_i \mid^2)^{\frac{1+\beta_2}{2}} \\ &- \sum_{i=0}^{\mathcal{N}}\frac{\mathcal{K}_{6i}}{(\frac{1}{2}\lambda_{\min}\{\mathcal{P}_{Mi}^{-1}\})^{\frac{1+\beta_1}{2}}}(\frac{1}{2}\lambda_{\min}\{\mathcal{P}_{Mi}^{-1}\}\|\tilde{\mathcal{W}}_{Mi}\|^2)^{\frac{1+\beta_1}{2}} \\ &- \sum_{i=0}^{\mathcal{N}}\frac{\mathcal{K}_{7i}}{(\frac{1}{2}\lambda_{\min}\{\mathcal{P}_{Mi}^{-1}\})^{\frac{1+\beta_2}{2}}}(\frac{1}{2}\lambda_{\min}\{\mathcal{P}_{Mi}^{-1}\}\|\tilde{\mathcal{W}}_{Mi}\|^2)^{\frac{1+\beta_2}{2}} \\ &- \sum_{i=0}^{\mathcal{N}}\frac{\mathcal{K}_{8i}}{(\frac{1}{2}\lambda_{\min}\{\mathcal{P}_{Ci}^{-1}\})^{\frac{1+\beta_1}{2}}}(\frac{1}{2}\lambda_{\min}\{\mathcal{P}_{Ci}^{-1}\}\|\tilde{\mathcal{W}}_{Ci}\|^2)^{\frac{1+\beta_1}{2}} \\ &- \sum_{i=0}^{\mathcal{N}}\frac{\mathcal{K}_{9i}}{(\frac{1}{2}\lambda_{\min}\{\mathcal{P}_{Ci}^{-1}\})^{\frac{1+\beta_2}{2}}}(\frac{1}{2}\lambda_{\min}\{\mathcal{P}_{Ci}^{-1}\}\|\tilde{\mathcal{W}}_{Ci}\|^2)^{\frac{1+\beta_2}{2}} \\ &- \sum_{i=0}^{\mathcal{N}}\frac{\mathcal{K}_{10i}}{(\frac{1}{2}\lambda_{\min}\{\mathcal{P}_{Gi}^{-1}\})^{\frac{1+\beta_1}{2}}}(\frac{1}{2}\lambda_{\min}\{\mathcal{P}_{Gi}^{-1}\}\|\tilde{\mathcal{W}}_{Gi}\|^2)^{\frac{1+\beta_1}{2}} \\ &- \sum_{i=0}^{\mathcal{N}}\frac{\mathcal{K}_{11i}}{(\frac{1}{2}\lambda_{\min}\{\mathcal{P}_{Gi}^{-1}\})^{\frac{1+\beta_2}{2}}}(\frac{1}{2}\lambda_{\min}\{\mathcal{P}_{Gi}^{-1}\}\|\tilde{\mathcal{W}}_{Gi}\|^2)^{\frac{1+\beta_2}{2}} \\ &+ \zeta_2 \\ \leq& -\varphi_2\mathcal{V}^{\frac{1+\beta_1}{2}} - \varphi_3\mathcal{V}^{\frac{1+\beta_2}{2}} + \zeta_2\end{aligned} \tag{34}$$

where $\varphi_2 = \min\left\{\frac{\lambda_{\min}\{\mathcal{K}_3\}}{(\frac{1}{2}\lambda_{\min}\{\mathcal{M}_a\})^{\frac{1+\beta_1}{2}}}, \frac{\mathcal{K}_{6i}}{(\frac{1}{2}\lambda_{\min}\{\mathcal{P}_{Mi}^{-1}\})^{\frac{1+\beta_1}{2}}}, \frac{\mathcal{K}_{8i}}{(\frac{1}{2}\lambda_{\min}\{\mathcal{P}_{Ci}^{-1}\})^{\frac{1+\beta_1}{2}}}, \frac{\mathcal{K}_{10i}}{(\frac{1}{2}\lambda_{\min}\{\mathcal{P}_{Gi}^{-1}\})^{\frac{1+\beta_1}{2}}}\right\}$, $\varphi_3 = \min\left\{\frac{\lambda_{\min}\{\mathcal{K}_4\}\mathcal{N}^{\frac{1-\beta_2}{2}}}{(\frac{1}{2}\lambda_{\min}\{\mathcal{M}_a\})^{\frac{1+\beta_2}{2}}}, \frac{\mathcal{K}_{7i}\mathcal{N}^{\frac{1-\beta_2}{2}}}{(\frac{1}{2}\lambda_{\min}\{\mathcal{P}_{Mi}^{-1}\})^{\frac{1+\beta_2}{2}}}, \frac{\mathcal{K}_{9i}\mathcal{N}^{\frac{1-\beta_2}{2}}}{(\frac{1}{2}\lambda_{\min}\{\mathcal{P}_{Ci}^{-1}\})^{\frac{1+\beta_2}{2}}}, \frac{\mathcal{K}_{11i}\mathcal{N}^{\frac{1-\beta_2}{2}}}{(\frac{1}{2}\lambda_{\min}\{\mathcal{P}_{Gi}^{-1}\})^{\frac{1+\beta_2}{2}}}\right\}$. ζ_2 can be proven to be bounded according to *Remark 1*.

The form of (34) is in keeping with *Lemma 1*. Therefore, the system state will arrive at the switching manifold (i.e. $\mathcal{S} = 0$) within a designed settling time $\mathcal{T}_1$, where

$$\mathcal{T}_1 = \frac{1}{\varphi_2}\frac{2}{1-\beta_1} + \frac{1}{\varphi_3}\frac{2}{\beta_2 - 1} \tag{35}$$

and the result is irrelevant with the selection of the initial conditions.

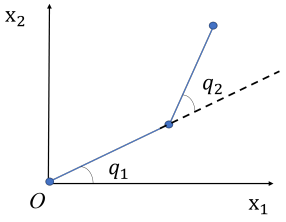

Fig. 1. Two-joint manipulator.

stage 2:

In this stage, the system state moves along the switching manifold. According to (20), we can obtain $\mathcal{S} = \dot{e} + \mathcal{K}_1\mathcal{H}(e) + \mathcal{K}_2\mathcal{S}\mathrm{sgn}^{\alpha}(e) = 0$.

When $\mid e_i \mid > \vartheta$, the dynamics of the tracking error e_i becomes

$$\dot{e}_i = -\mathcal{K}_{1i}\,\mathrm{sgn}^{\rho}(e_i) - \mathcal{K}_{2i}\,\mathrm{sgn}^{\alpha}(e_i) \tag{36}$$

where $\mathcal{K}_{1i}$ and $\mathcal{K}_{2i}$ denote the diagonal elements of matrices $\mathcal{K}_1$ and $\mathcal{K}_2$, respectively. Define the Lyapunov function as $\mathcal{V}_1 = e_i^2$. Taking the first derivative of $\mathcal{V}_1$ yields:

$$\dot{\mathcal{V}}_1 = -2\mathcal{K}_{1i}\left(e_i^2\right)^{\frac{1+\rho}{2}} - 2\mathcal{K}_{2i}\left(e_i^2\right)^{\frac{1+\alpha}{2}} \tag{37}$$

It is obvious that (37) is consistent with (12), which means the tracking error e_i can convergence to a small domain $\Omega = \{e_i | \mid e_i \mid \leq \vartheta\}$ within the designed settling time $\mathcal{T}_2$ and

$$\mathcal{T}_2 = \frac{1}{\mathcal{K}_{1i}}\frac{1}{1-\rho} + \frac{1}{\mathcal{K}_{2i}}\frac{1}{\alpha-1} \tag{38}$$

When $\mid e_i \mid \leq \vartheta$, based on (17) the dynamics of the tracking error e_i changes to

$$\dot{e}_i = -\mathcal{K}_{1i}\left(\phi\,\mathrm{sgn}^{\rho+1}(e_i) + \psi\vartheta^{|e_i|}e_i\right) - \mathcal{K}_{2i}\,\mathrm{sgn}^{\alpha}(e_i) \tag{39}$$

Construct the Lyapunov function candidate $\mathcal{V}_2 = \frac{1}{2}e_i^2$. Differentiating $\mathcal{V}_2$ with respect to time yields

$$\dot{\mathcal{V}}_2 = -\mathcal{K}_{1i}\phi \mid e_i \mid^{\rho+2} -\mathcal{K}_{1i}\psi\vartheta^{|e_i|}e_i^2 - \mathcal{K}_{2i} \mid e_i \mid^{\alpha+1} \tag{40}$$

Since $0 < \vartheta < \exp(-1)$, $\rho = 1-\vartheta$, we can derive that $\phi > 0$ and $\psi > 0$ based on (17). Therefore, we can obtain $\dot{\mathcal{V}}_2 < 0$, which means the system state can asymptotically converge to the origin. This completes the proof. ■

IV. Simulation

In this section, two simulation studies are given to prove the effectiveness of the proposed method. The first one is to compare the convergence effect of the proposed non-singular fixed-time controller and the general TSM controller in [9]. The other is to verify the performance of the manipulator when it interacts with the environment under the control of the proposed controller. The simulation plant is a two-joint manipulator shown as Fig.1, which is given by the parameters in the dynamics

$$\mathcal{M}_a = \begin{bmatrix}\mathcal{M}_{11} & \mathcal{M}_{12}\\ \mathcal{M}_{21} & \mathcal{M}_{22}\end{bmatrix} \quad \mathcal{C}_a = \begin{bmatrix}\mathcal{C}_{11} & \mathcal{C}_{12}\\ \mathcal{C}_{21} & \mathcal{C}_{22}\end{bmatrix} \quad \mathcal{G}_a = \begin{bmatrix}\mathcal{G}_1\\ \mathcal{G}_2\end{bmatrix}$$

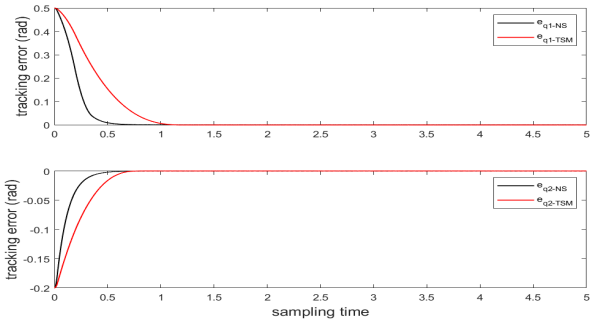

Fig. 2. Comparison of the angle tracking errors in two controllers.

where $\mathcal{M}_{11} = \mathcal{L}(1) + \mathcal{L}(2) + 2\mathcal{L}(3)\cos(q_2)$, $\mathcal{M}_{12} = \mathcal{M}_{21} = \mathcal{L}(2) + \mathcal{L}(3)\cos(q_2)$, $\mathcal{M}_{22} = \mathcal{L}(2)$, $\mathcal{C}_{11} = -\mathcal{L}(3)\dot{q}_2\sin(q_2)$, $\mathcal{C}_{12} = -\mathcal{L}(3)(\dot{q}_1+\dot{q}_2)\sin(q_2)$, $\mathcal{C}_{21} = \mathcal{L}(3)\dot{q}_1\sin(q_2)$, $\mathcal{C}_{22} = 0$, $\mathcal{G}_1 = \mathcal{L}(4)g\cos(q_1) + \mathcal{L}(5)g\cos(q_1+q_2)$, $\mathcal{G}_2 = \mathcal{L}(5)g\cos(q_1+q_2)$, $\mathcal{L} = [2.9; 0.76; 0.87; 3.04; 0.87]$, g is the gravitational acceleration. To achieve fast convergence and small tracking error, the parameters in the control torque are finally tuned as $\vartheta = 0.3$, $\rho = 0.7$, $\alpha = 1.9$, $\mathcal{K}_1 = \mathcal{K}_2 = \mathcal{K}_5 = [5\ 0; 5\ 0]$, $\mathcal{K}_3 = [50\ 0; 50\ 0]$, $\mathcal{K}_4 = [2\ 0; 5\ 0]$, $\mathcal{K}_6 = [0.01\ 0; 0.01\ 0]$, $\beta_1 = 0.5$, $\beta_2 = 2$.

A. Comparison Study

This simulation setup is to track the same joint angle, where the desired joint angles are set as $q_{r1} = 0.6$ and $q_{r2} = 1.7$. The initial values of the joints are selected as $q_1(0) = 1.1$, $q_2(0) = 1.5$, $\dot{q}_1(0) = \dot{q}_2(0) = 0$. The curves of the angle tracking errors are shown in Fig.2, where the label $-_{NS}$ and $-_{TSM}$ in the legend represent the non-singular fixed-time controller and the general TSM controller, respectively. It is obvious that both controllers can converge the angle tracking error, and the system using the non-singular fixed-time controller has faster convergence effect than that using the general TSM controller.

B. Manipulator Interacting With Environment

In this simulation, the admittance model is utilized to modify the reference trajectory, and the proposed fixed-time controller is employed for angle tracking. The parameters in the dynamic model are approximated by BRFNN. An external torque will be exerted on the manipulator from sampling time 8 to 16, where $\tau_e = [2; 0]$. The original reference trajectory is designed as $q_{d1} = 1.25 - \frac{7}{5}\exp(-t) + \frac{7}{20}\exp(-4t)$, $q_{d2} = 1.25 + \exp(-t) - \frac{1}{4}\exp(-4t)$. We set the external disturbance as $[2\sin(0.2t); \cos(0.5t) + 0.5\sin(0.1\pi t)]$. The initial values of the joints are selected as $q_1(0) = 0.6$, $q_2(0) = 1.8$, $\dot{q}_1(0) = \dot{q}_2(0) = 0$. The parameters in the admittance model are chosen as $\mathcal{D}_A = [3\ 0; 3\ 0]$, $\mathcal{C}_A = [30\ 0; 30\ 0]$ and $\mathcal{G}_A = [20\ 0; 20\ 0]$. By balancing the computing time and the approximate effect, the RBFNNs are designed with 5 neurons and their parameters are chosen as $\sigma_{\mathcal{M}} = \sigma_{\mathcal{C}} = \sigma_{\mathcal{G}} = [-1; -0.5; 0; 0.5; 1]$, $\varrho_{\mathcal{M}} = \varrho_{\mathcal{C}} = \varrho_{\mathcal{G}} = 10$, $\varepsilon_{\mathcal{M}i} = 2$, $\varepsilon_{\mathcal{C}i} = 0.55$, $\varepsilon_{\mathcal{G}i} = 0.05$, $\mathcal{P}_{\mathcal{M}ii} = 15$, $\mathcal{P}_{\mathcal{C}ii} = 10$, $\mathcal{P}_{\mathcal{G}ii} = 25$. The simulation results are

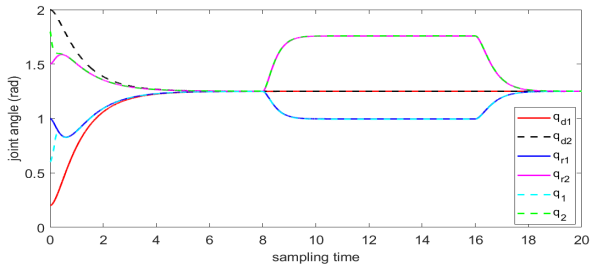

Fig. 3. Trajectory tracking with admittance control.

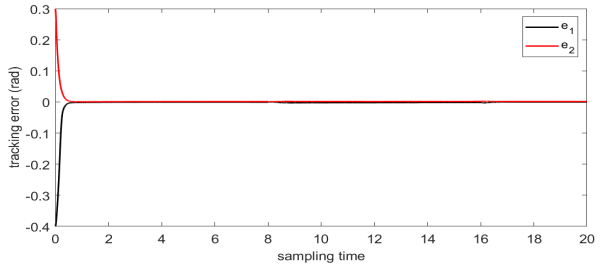

Fig. 4. Tracking errors.

shown as Figs. 3-5, where q_i is the real-time angle of the i-th joint of the manipulator, q_{di} represents the original reference joint angle, q_{ri} denotes the modified joint angle by admittance model. In the beginning, the modified trajectory gradually coincides with the reference trajectory, which is consistent with the admittance model that when $f_{ext} = 0$, $q_r \rightarrow q_d$. Then, a large change of the modified trajectory occurs because of the external torque. The external torque is canceled after sampling time 16, therefore, the modified trajectory gradually coincides with the reference trajectory again. We set an input constrain as 50 N$*$m for safety, that is why the control torque is limited to 50 N$*$m at the beginning. During the whole process, the manipulator can quickly track the modified trajectory even though there is a large variation in the trajectory.

V. Conclusion

In this paper, we propose a non-singular fixed-time controller for unknown-dynamics manipulators. An admittance model is adopted into the system to realize compliant behavior of the manipulator while interacting with environment.

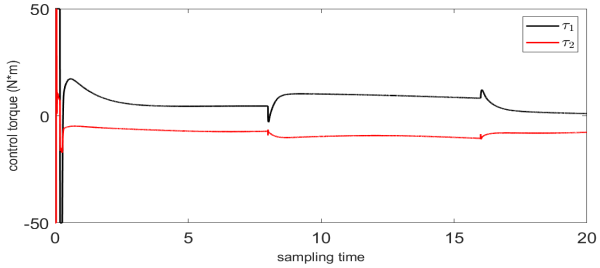

Fig. 5. Control torques.

The sliding mode control based on a non-singular fixed-time switching manifold is introduced to the system control design, which greatly improves the convergence effect of the system. In addition, RBFNNs are employed to approximate the unknown parameters in the dynamics. Simulation studies verify that the proposed controller has better tracking error convergence and faster response to external interaction than that using the traditional terminal sliding mode method.

References

[1] P. Xu, C.-F. Cheung, B. Li, et al., "Kinematics analysis of a hybrid manipulator for computer controlled ultra-precision freeform polishing," Robot. Comput. Integr. Manuf., vol. 44, pp. 44–56, 2017.

[2] C. Shin, P. W. Ferguson, S. A. Pedram, et al., "Autonomous tissue manipulation via surgical robot using learning based model predictive control," Int. Conf. Robot. Autom., pp. 3875–3881, 2019.

[3] M. Schumacher, J. Wojtusch, P. Beckerle, O. Stryk, "An introductory review of active compliant control," Robot. Auton. Syst., vol. 119, pp. 185–200, 2019.

[4] M. T. Mason, "Compliance and force control for computer controlled manipulators," IEEE Trans. Syst., Man, Cybern., vol. 11, no. 6, pp. 418–432, 1981.

[5] C. Yang, G. Peng, Y. Li, et al., "Neural networks enhanced adaptive admittance control of optimized robotenvironment interaction," IEEE Trans. Cybern., vol. 49, no. 7, pp. 2568–2579, 2019.

[6] G. Peng, C. L. P. Chen and C. Yang, "Neural networks enhanced optimal admittance control of robot-environment interaction using reinforcement learning," IEEE Trans. Neural Netw. Learn. Syst., pp. 1–11, 2021.

[7] Y. Li, C. Yang, W. Yan, et al., "Admittance-based adaptive cooperative control for multiple manipulators with output constraints," IEEE Trans. Neural Netw. Learn. Syst., vol. 30, no. 12, pp. 3621-3632, 2019.

[8] W. He, C. Xue, X. Yu, et al., "Admittance-based controller design for physical humanrobot interaction in the constrained task space," IEEE Trans. Autom. Sci. Eng., vol. 17, no. 4, pp. 1937-1949, 2020.

[9] Y. Wu, X. Yu, and Z. Man, "Non-singular terminal sliding mode control of rigid manipulators," Autom., vol. 38, no. 12, pp. 2159–2167, 2002.

[10] S. Sivrioglu and K. Nonami, "Sliding mode control with time-varying hyperplane for AMB systems," IEEE/ASME Trans. Mechatronics, vol. 3, no. 1, pp. 51–59, 1998.

[11] Y. Tang, "Terminal sliding mode control for rigid robots," Autom., vol. 34, no. 1, pp. 51–56, 1998.

[12] Z. Man and X. Yu, "Terminal sliding mode control of MIMO linear systems," IEEE Trans. Circuits Syst. I, vol. 44, no. 11, pp. 1065–1070, 1997.

[13] Y. Wu, X. Yu, and Z. Man, "Terminal sliding mode control design for uncertain dynamic systems," Syst. Control Lett., vol. 34, no. 5, pp. 281–287, 1998.

[14] L. Zhang, Y. Wang, Y. Hou and H. Li, "Fixed-time sliding mode control for uncertain robot manipulators," IEEE Access, vol. 7, pp. 149750-149763, 2019.

[15] B. Jin, "Robotic manipulator trajectory control using neural networks," Proc. Inst. Conf. Neural Netw., vol. 2, pp. 1793–1796, 1993.

[16] G. Peng, C. Yang, W. He, et al., "Force sensorless admittance control with neural learning for robots with actuator saturation," IEEE Trans. Ind. Electron., vol. 67, no. 4, pp. 3138–3148, 2020.

[17] G. Peng, C. L. P. Chen, W. He and C. Yang, "Neural-learning-based force sensorless admittance control for robots with input deadzone," IEEE Trans. Ind. Electron., vol. 68, no. 6, pp. 5184–5196, 2021.

[18] A. Polyakov, "Nonlinear feedback design for fixed-time stabilization of linear control systems," IEEE Trans. Autom. Control, vol. 57, no. 8, pp. 2106–2110, 2012.

[19] B. Jiang, Q. Hu and M. I. Friswell, "Fixed-time attitude control for rigid spacecraft with actuator saturation and faults," IEEE Trans. Control Syst. Technol., vol. 24, no. 5, pp. 1892-1898, 2016.

[20] Z. Zuo and L. Tie, "A new class of finite-time nonlinear consensus protocols for multi-agent systems," Int. J. Control, vol. 87, no. 2, pp. 363-370, 2014.

[21] C. D Rahn, Mechatronic Control of Distributed Noise and Vibration: A Lyapunov Approach. Heidelberg, Germany: Springer-Verlag, 2001.